Preliminary aero-mechanical jitter analysis of hemispherical turrets

Timothy J. Bukowski*[a], R. Mark Rennie[a], Stanislav Gordeyev[a], and Matthew Kemnetz[b]

[a]University of Notre Dame, Notre Dame, Indiana, 46556
[b]U.S. Air Force Research Laboratory, Kirtland Air Force Base, New Mexico, 87117

ABSTRACT

This work presents preliminary results on aero-mechanical jitter of a hemispherical optical turret. A simplified geometry with a hemispherical shell and optics-holding canister was designed to reduce degrees of freedom and provide better insight into fundamental physics. Modal analysis of the turret and mounting plate to the wind tunnel, performed using finite element analysis (FEA), revealed significant plate displacements in the lowest frequency modes. Three mounting plate thicknesses (1/4", 1/2", and 1") were tested. Wind tunnel tests at the University of Notre Dame's White Field Mach 0.6 wind tunnel assessed turret vibrations at speeds from Mach 0.2 to 0.5, using accelerometers and Shack-Hartmann tilt sensors. Two scenarios were tested: one with the turret inside the tunnel exposed to the flow, and another with the turret attached outside of the wind tunnel so that it is only excited by the base motion of the wind tunnel. The 1/4" plate showed tilt measurements ranging from 30 to 190 microradians when exposed to flow, compared to 10 to 50 microradians in the baseline case. The 1/2" and 1" plates exhibited lower tilts and less distinction between flow and baseline conditions. Overall, the simplified turret only had about three vibration modes affecting tilt, with strong spatial agreement between experimental and FEA modal patterns.

Keywords: jitter, hemispherical turret, vibration, wind tunnel, finite element analysis,aerodynamic forcing

1. INTRODUCTION

There is considerable interest in airborne laser systems and much research has been done to make these feasible.[1–4] Hemispherical turrets are a popular beam director design due to their simple geometry and wide field of regard. However, protruding these blunt bodies from the aircraft into the flow creates significant aerodynamic disturbance and a strong unsteady wake. A diagram in Fig. 1 shows some of the main flow features.[5] This flow field has been studied in depth in wind tunnel tests,[6–10] flight tests,[6,11–13] and computational fluid dynamics (CFD)[14,15] and the fluid dynamics is fairly well understood.[16] The complicated wake behind the turret degrades a beam-propagation system's performance in two ways. First, it creates density fluctuations which will lead to aberrations in the beam wavefront.[16] Second, the unsteady pressure field shakes the turret, which in turn shakes the optical components in the turret and leads to beam jitter. While the aerodynamics and aero-optics are fairly well understood,[17,18] the mechanical response of the optical train to the unsteady aerodynamics is complex. Work has been done to show general relations between the pressure field and jitter. De Lucca et al. related beam jitter to the unsteady pressure field and showed the contribution of different features of the turret.[19–21] Mechanical jitter of the Airborne Laser Laboratory (ALL) was also studied.[22] Specific cases have had success in modeling and predicting system jitter levels. Griffin et al. outlined the Line-of-Sight jitter modeling of the advanced tactical laser (ATL) system where the measured system closed-loop jitter was close to predictions.[23] Merritt outlined how local loop jitter can be estimated from system vibration measurements.[24] To investigate potential aeroelastic effects on the wake of a turret, Roeder and Gordeyev conducted experiments to examine the fluid-structure interaction of a turret in subsonic flow.[25] Their study showed that when the turret is allowed to oscillate due to unsteady flow forces, the resulting changes in the wake are minimal, even with relatively large oscillations (approximately 1 mm or 0.2 of the turret radius). Given that turret motion in practical applications

*Further author information:
E-mail: tbukowski@nd.edu, Telephone: (574) 631-4280

Unconventional Imaging, Sensing, and Adaptive Optics 2024, edited by Jean J. Dolne, Santasri R. Bose-Pillai, Matthew Kalensky, Proc. of SPIE Vol. 13149, 131490E
© 2024 SPIE · 0277-786X · doi: 10.1117/12.3028193

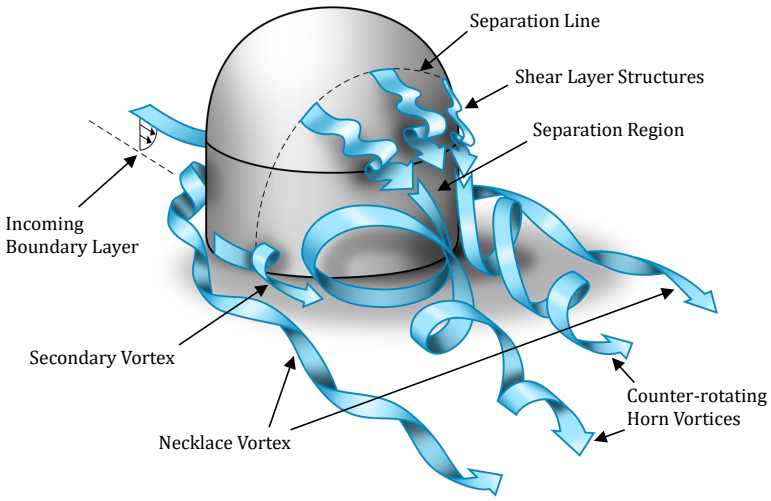


Figure 1: Sketch of main flow features in flow over a hemispherical turret. Figure reproduced from Kalensky et. al. 2024 with permission.[5]

is usually less significant, these findings imply that aeroelastic effects can be neglected when analyzing the wake dynamics and the associated unsteady forces on the turret.

The aeromechanical jitter resulting from this shaking is a difficult multidisciplinary problem that additionally involves the dynamic response of the mechanical structure, the behavior of the optical system, and the coupling between all these elements. Unfortunately, jitter analyses are typically performed for complicated optical configurations or prototype beam directors that are close to final, deployed systems. Even the AAOL turret used in the study described above had a coude path with around 20 distinct optical elements including windows, mirrors, lenses, and other components.[24,26,27] In the work presented here, we use a simplified turret design with significantly reduced degrees of freedom which should allow us to uncover and model relationships, mechanisms, and fundamental physics. In what follows, we first go through the experimental setup and design of the simple turret geometry. Section 3 shows the vibration modes of the model and how we were able to measure and visualize these modes in experiment. Then in Section 4 we show tilt results from wind tunnel testing. In the final Section 5 we summarize our results.

2. TEST MODEL DESIGN

The geometry used here is a simple 1/8" aluminum hemispherical shell that has an optical canister holding a mirror and a lens that is conformal to the turret surface. The canister is designed to perform as an optical flat, where the collimated laser beam entering the canister along the axis is reflected back as a collimated beam.[4] The hemisphere has an outer diameter of 10" and the canister mirror has an aperture diameter of 2". The turret is bolted to an aluminum mounting plate which fits into the wind tunnel test section floor. Plate thicknesses of 1/4", 1/2", and 1" were tested. The materials used for each component are listed in Table 1. An exploded view of the turret is shown in Fig. 2.

3. MODAL ANALYSIS

We first performed modal analysis to determine resonant frequencies and mode shapes for the model. Based on past surface pressure field data, we expect variations in the frequency range below a non-dimensional frequency, or Strouhal number of 0.5, where $St_D = \frac{fD}{U}$ with frequency f, hemisphere diameter D, and freestream velocity U.[25] For Mach numbers from 0.3 to 0.6 in the wind tunnel, $St_D = 0.5$ corresponds to a frequency of around 200-410 Hz. We also expect a strong peak in the spectra from vortex shedding around $St_D = 0.2$ which would correspond to frequencies around 80-160 Hz.[25] An example of spectra from integrated surface pressure data for different Mach numbers is shown in Fig. 3.

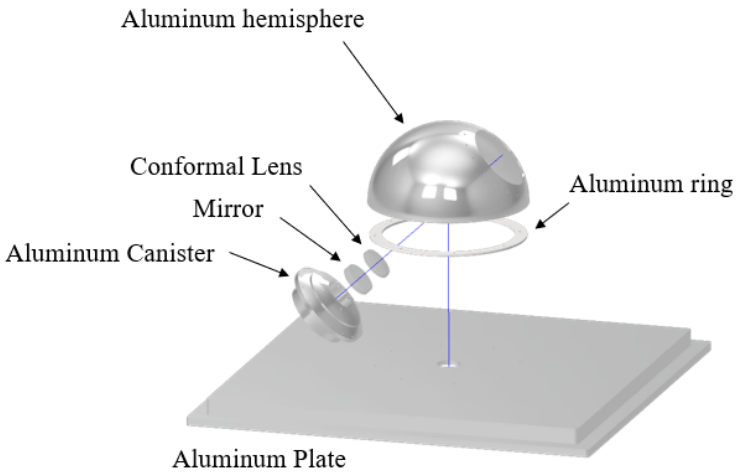


Figure 2: Exploded view of turret components and the plate that connects the turret to the wind tunnel.

Part	Material
Hemisphere Shell	Al 3003-O
Ring	Al 6061-T6
Lens	Fused Silica
Mirror	Fused Silica
Canister	Al 6061-T6
Plate	Alca 5 (AA5083)

Table 1: Materials

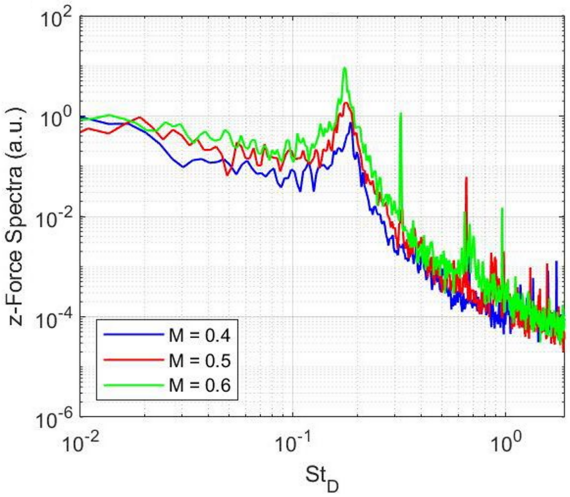


Figure 3: Spanwise force spectra for a hemispherical turret. Figure reproduced from Roeder et. al. 2022 with permission.[25]

In the modal analysis, we were looking for low-frequency modes below 200 Hz that could be excited by the flow and therefore cause significant tip/tilt. This analysis also allowed us to visualize the mode shapes to better understand what would be causing the motion.

3.1 Finite Element Analysis

Vibration modes were solved with finite element analysis using Ansys Mechanical. A zero displacement boundary condition was applied around the edge of the plate, where it is bolted to the wind tunnel. The leading modes are shown in Fig. 4. A significant takeaway is that most of the motion of the model mirror is associated with the deformation of the mounting plate, with negligible deformation of the turret itself. Further, the modes of the plate with the canister mounted look very similar to the modes of the plate without the canister. For the 1/4" plate the first mode has a frequency of 127 Hz and has a shape in which the center of the plate oscillates up and down like a drum. The next two modes are at 228 Hz and 239 Hz with the two modes having the turret rocking in orthogonal directions. The 228 Hz mode has a lower frequency due to the higher moment of inertia from the canister which would be moving up and down, whereas in the higher frequency 239 Hz mode, the canister is mostly just rotating. The next set of modes oscillate at frequencies from 688 Hz to 792 HZ with displacement mainly at the corners of the plate. The higher frequency vibration of these modes leads to lower amplitude displacements, and from the mode shapes, we see there is less motion of the turret relative to the other modes, so these modes will not contribute much to tip/tilt in the beam. Higher modes exist, but will not be excited enough to add to beam jitter. The same analysis was done for the other thicker plates finding very similar mode shapes, just at higher frequencies. For the 1/2" plate the first three modes have frequencies around double those of the 1/4" plate at 268, 476, and 500 Hz. For the 1" plate the natural frequencies are just under double those of the 1/2" plate at 500, 808, and 866 Hz. This analysis helped in the design process as we decided on the materials and sizing of different parts.

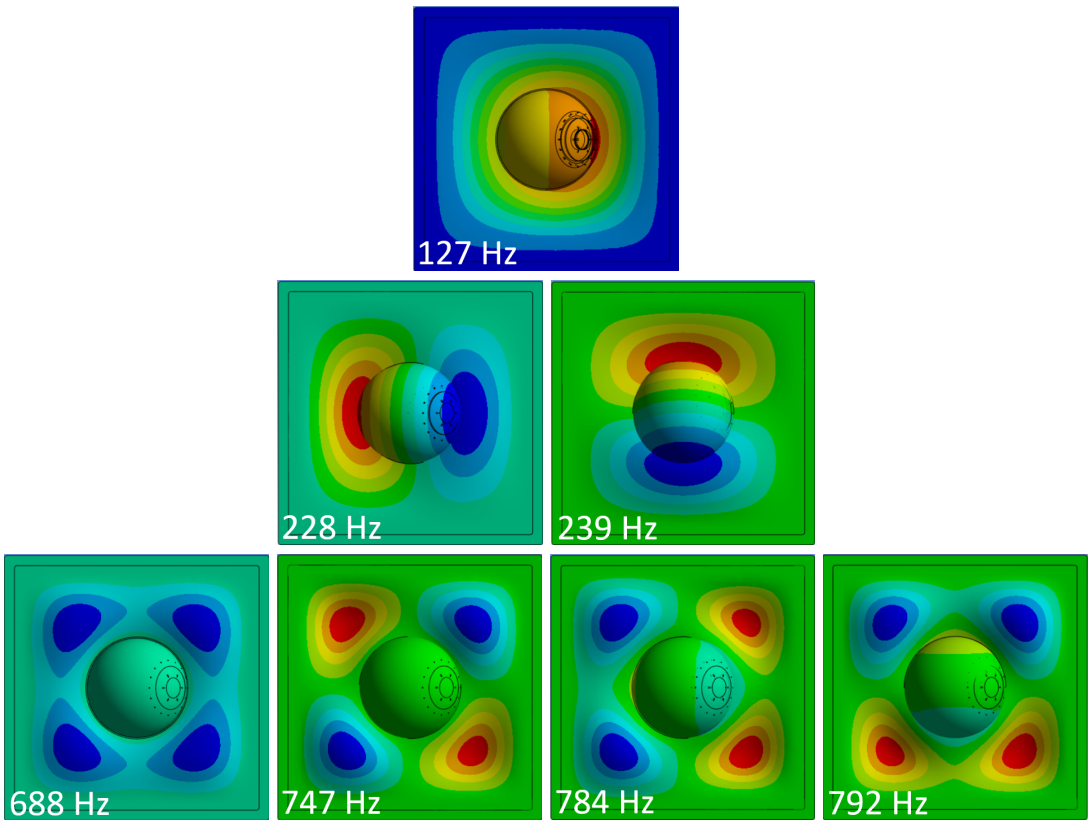


Figure 4: Vibration modes of the plate and turret assembly up to 914 Hz.

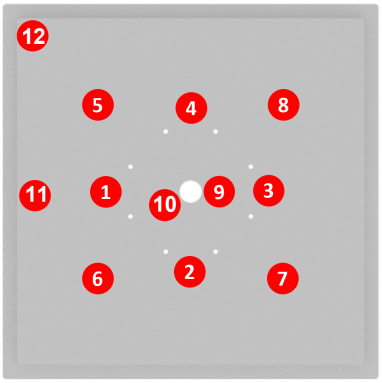


Figure 5: Location of accelerometers used for impact excitation testing. The canister is facing towards sensor 3. Wind tunnel flow direction goes from top to bottom.

3.2 Impact Excitation

Once the turret and plates were manufactured, impact excitation tests were performed to measure the vibration modes of the constructed turret, and to compare with the modes found in simulation. We did these tests on individual components as we put things together so we could see which parts were modeled correctly. This way, we could pinpoint which part or connection was not properly modeled. For the impact tests, twelve PCB accelerometers were placed around the plate as shown in Fig. 5, where the canister is facing sensor 3. The accelerometers were placed close to the peaks of the vibration modes shown in Fig. 4, with sensors 11 and 12 placed at the edge of the plate to monitor the boundary motion and to see how close to a fixed boundary condition it is. The turret and plate were installed in the wind tunnel and tapped with a plastic mallet repeatedly in different locations on the plate for a total of about 10 taps, waiting for the ringing to dampen out between taps. The acceleration spectra from the accelerometer measurements were pre-multiplied by frequency to emphasize the peaks and are shown in Fig. 6. Here we see the lowest frequency peak at 117 Hz, with a pair of peaks at 216 Hz and 231 Hz. Another cluster of higher frequency peaks appears at 610, 711, and 774 Hz. While these peaks are lower than the simulation mode frequencies, their grouping is similar, suggesting that the 117 Hz peak corresponds to the drumming mode, the 200 Hz modes are the pitching and rolling modes, and the 600-700 Hz modes are the corner modes. Additionally, by relating the amplitudes of the peaks to the spatial locations of their sensors, we can see that the 117 Hz mode is most excited at sensors 9 and 10 in the center of the plate which matches the 127 Hz mode found in simulation. The 216 Hz peak is excited at all corner sensors 5-8 and also at side sensors 1 and 3, but not 2 and 4 matching with the 228 Hz pitching mode from simulation. The 231 Hz peak is excited at all corner sensors 5-8 and also at side sensors 1 and 3, but not 2 and 4 matching with the 239 Hz rolling mode from simulation. Then the 610-774 Hz set of peaks are only excited for sensors 5-10 which matches higher frequency corner modes from simulation. The same tests were done for the thicker plates, however, the peaks were not as clear and it was difficult to extract the modal frequencies. Further work will be done to determine these.

3.3 Extraction of Modes

To further visualize the modes excited by the impact tests, we plotted the real component of the Fourier coefficient on a spatial plane shown in Fig. 7 for the first three peak frequencies from Fig. 6. Constant zero values were added to the edge of the plate where there were no accelerometers and values were interpolated between all of the point measurements to create a spatial map of the Fourier mode. We can see that the modes look quite similar to those shown in Fig. 4.

A phase shift can be added to create a video of the modes. When this was done we noticed other motion in the 216 and 231 Hz modes which looked like the peak was moving in a circle, suggesting there may be multiple modes superimposed. To separate the modes a spectral version of proper orthogonal decomposition (SPOD) was

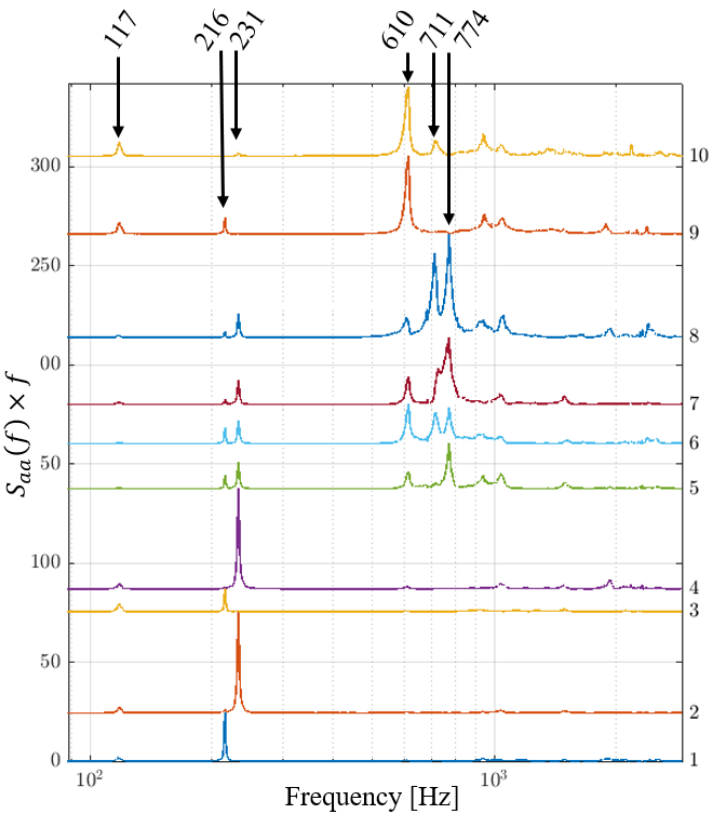


Figure 6: Pre-multiplied spectra for accelerometers 1-10.

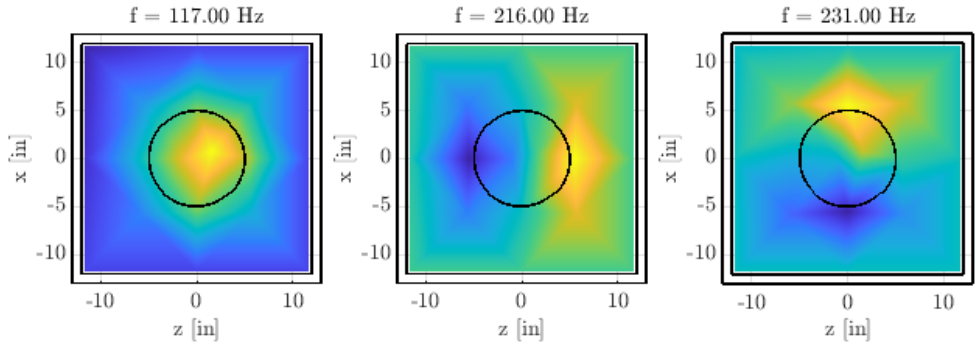


Figure 7: Fourier modes at first three peak frequencies.

used.[28] Here, POD is performed in the spectral domain, decomposing each Fourier mode $\hat{a}_k$

$$a(\mathbf{x},t) \xrightarrow{\mathcal{F}} \hat{a}(\mathbf{x},f) \tag{1}$$

$$\hat{a}_(\mathbf{x},f) = \sum_{n=1}^{\infty} c_n(f)\phi_n(\mathbf{x},f) \tag{2}$$

where a is the measured acceleration with the mean removed, $\mathbf{x}$ is the three dimensional spatial coordinate, ϕ_{kn} are the POD modes and c_{kn} are the corresponding spectral coefficients. The modes are calculated by solving the eigenvalue problem of the cross-spectral density matrix S.

$$S(\mathbf{x},\mathbf{x}',f) = \langle \hat{a}_(\mathbf{x},f)^* \hat{a}_(\mathbf{x},f) \rangle \tag{3}$$

$$\int_\Omega S(\mathbf{x},\mathbf{x}',f')\phi_n(\mathbf{x}',f')d\mathbf{x}' = \lambda_n(f')\phi_n(\mathbf{x},f') \tag{4}$$

where λ_n are the eigenvalues that give the energy of each mode and the angle brackets denote an ensemble average over statistically independent realizations. By construction, POD modes are orthonormal, $\int_s \phi_n(s)\phi_m(s)ds = \delta_{nm}$ where δ_{nm} is the Kronecker delta. The spectra coefficients can be found by projecting the Fourier coefficients $\hat{a}$ onto the modes as

$$c_n(f) = \int_\Omega \hat{a}(\mathbf{x},f)\phi_n(\mathbf{x},f)d\mathbf{x} \tag{5}$$

This decomposition was done using the Matlab code from Ref. 29. The real component of the first three SPOD modes for the first three peak frequencies are shown in Fig. 8. Here we see that the SPOD modes very closely match the FEA mode shapes shown in Fig. 4, with the 117 Hz mode 1 showing the drumming motion of the center of the plate, the 216 Hz mode having the rocking motion pitching the canister up and down, while the 232 Hz mode has an orthogonal rocking motion rolling the turret canister. Mode 2 for 216 Hz shows the rolling mode, while mode 2 for 231 Hz shows the pitching mode, however, mode 2 for 117 Hz does not show a discernible vibration mode. Mode 3 at 117 Hz looks similar to the rocking modes, while mode 3 at 216 and 231 Hz look similar to the drum mode. However, these modes are very low energy.

This modal analysis was important to ensure that the finite element model of the turret and plate matches the measured data from the experiment. Material properties between the different components were matched as best as possible. The weights of the components are within 3% of the weight estimated in simulation.

Experimental measurement of the modal shapes was very important to this analysis as early FEA calculations of the vibration modes had the lowest frequency drumming mode at around 250 Hz with the rolling modes at 450 Hz. However, the SPOD analysis showed for certain that the 117 Hz mode was in fact the drumming mode, demonstrating that the FEA model needed to be updated. Further work showed that the errors in the FEA modeling could be traced to insufficient mesh resolution of small features, specifically, the small bolts and holes associated with fastening the optical canister to the hemispherical turret. One objective of this research is to determine if numerical aero-mechanical jitter computations can produce sufficiently accurate results without the need for detailed modeling of these kinds of fine details. As such, we began investigating the FEA modeling with these bolts and holes eliminated. However, the bolt connection between the plate and turret was found to be important. When the plate was modeled as fully bonded to the ring on the bottom of the turret, there was too much stiffness added to the center of the plate and the drum and rocking modes had very high frequencies. We instead modeled the screw interface by bonding the plate to the turret at eight 1/4" circles where the screws are which lowered the frequencies of those first three modes by 20 Hz.

Another possible contributor to the experiment having lower natural frequencies is the boundary condition. In the wind tunnel, the edges of the plate do not have a true zero displacement condition, as the tunnel is not perfectly stiff. Further agreement could be found by modifying the boundary condition in the FEA analysis, but a better solution we found was to use a free boundary condition, where the plate is essentially vibrating in free space. We approximated this boundary condition for impact testing by holding the edge of the plate in one hand while tapping with the mallet. For the case of the plate without the turret, the modal frequencies were within 1% of the FEA prediction, suggesting that holding the plate is close to the free boundary condition. For

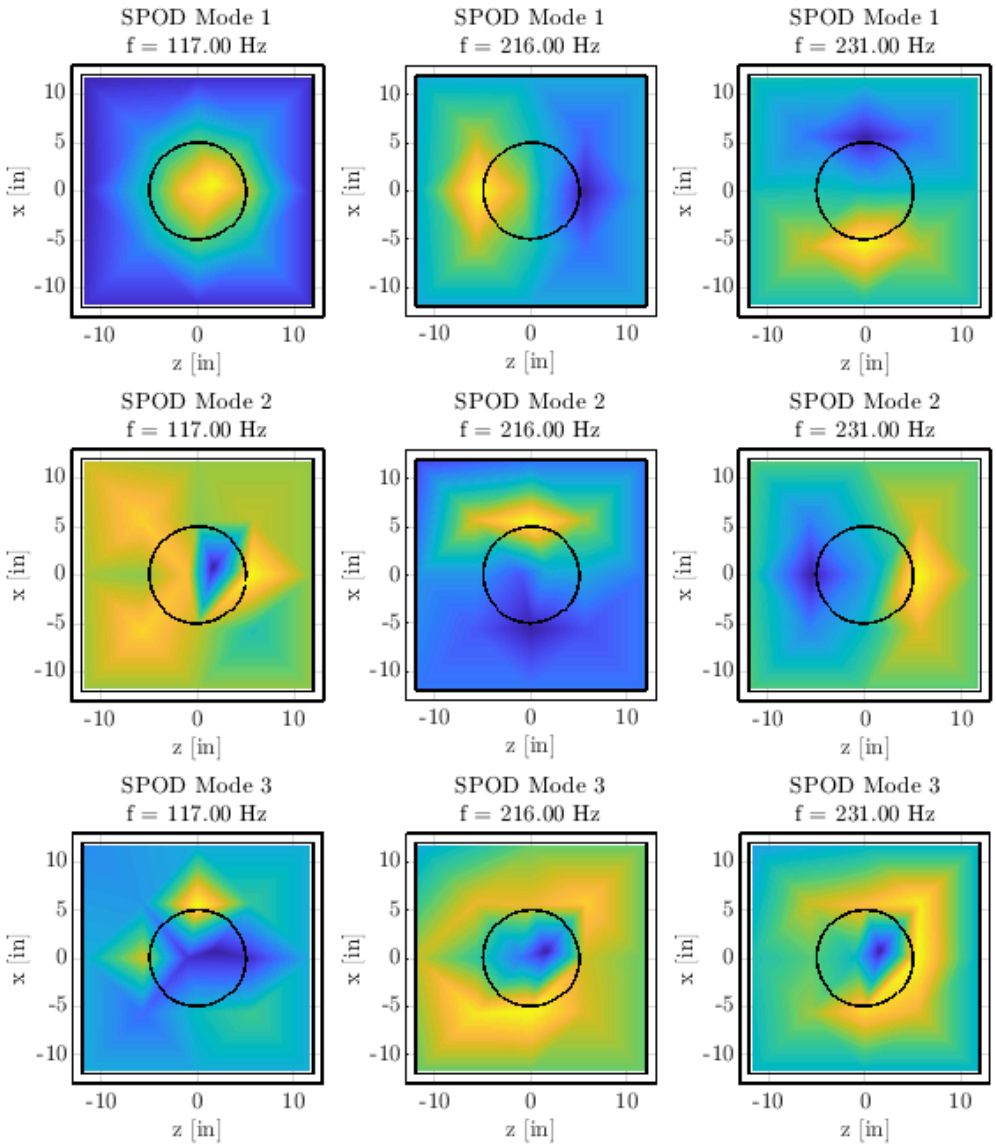


Figure 8: First three SPOD modes for the first three peak vibration frequencies.

the turret and plate, the experimentally measured frequencies were within 1% lower of the FEA prediction for the 1/4" plate, and within 3% for the 1/2" plate. For the 1" plate there was significant disagreement of over 10% between the experiment and FEA. Further work is needed to increase agreement for the thickest plate. The interface between the turret and the plate is likely the source of the discrepancy and further work is required to figure out how best to model this.

4. WIND TUNNEL MEAUSUREMENTS

4.1 Experimental Setup

Wind tunnel testing was performed at the University of Notre Dame's White Field Mach 0.6 wind tunnel. This wind tunnel has a 3 × 3 ft test section and data were collected at a freestream Mach numbers of 0.2 - 0.5 ($Re_D \approx 0.8 - 2 \times 10^6, U_\infty \approx 152 - 380$ mph). This facility is particularly useful as the dynamic pressures are similar to those seen in flight. Shack–Hartmann wavefront sensor (SHWFS) measurements were taken to obtain global and local tilts on the beam. A 532 nm Novanta opus laser source was used which was expanded to a 1" aperture then expanded again through an f400 and f800 lens to a 2" aperture beam that was reflected off the turret canister mirror and passed back through the telescope reducing it back to a one-inch beam. The mirror was then reimaged onto the SHWFS by a f250 and f200 lens, shrinking the beam to 0.8" aperture. SHWFS images were taken using a Phantom v1611 high-speed camera. Thirteen accelerometers were placed around the turret and plate in positions shown in Fig. 11 to provide vibration measurements. Accelerometers 1-12 were single-axis PCB 352C33 sensors and accelerometer 13 was a tri-axis PCB 356A14. Accelerometers 1-8 were read through a PCB 483C05 signal conditioner while 9-13 were read by PCB 482A22 signal conditioners. Five accelerometers were placed around the edge of the plate to capture the boundary condition of the plate. Two were placed towards the middle of the plate to capture vibration modes. The three-axis accelerometer was placed on the top of the turret to capture turret motion. Three accelerometers were placed on the canister for a redundant measurement of tilt. The final two sensors were placed on the optics tables. All data was collected at a sampling rate of 20 kHz and both data acquisition clocks and triggers were synced. Accelerometer data was recorded for 30 seconds and SHWFS data was recorded for about 2 seconds. Flow speed measurements were obtained using the dynamic pressure measured with a Pitot probe and a Setra 270 transducer at the entrance to the test section. The turret has an elevation angle of 43 degrees relative to the floor of the tunnel and an azimuthal angle of 90 degrees relative to the upstream direction. The 43 degree elevation angle was chosen to maximize usable azimuthal angles with optical access to send a beam to the canister mirror.

Two scenarios were tested for each plate thickness. The first was a case with the turret inside the tunnel. However, when the turret is in the tunnel, it is excited by both the flow and the base motion of the tunnel walls. As such, we also tested a second configuration where we mounted the turret to the outside of the tunnel with the wind tunnel running to capture the influence of just the base vibration on the turret jitter. By mounting the turret underneath the tunnel, we can retain very similar vibration modes and bounce a beam off the canister to measure tip tilt, while eliminating aerodynamic effects on the turret. Both of these scenarios were run for the 1/4", 1/2", and 1" plates.

4.2 Results

The global tilt across the beam was calculated by taking the spatial average of the SHWFS measured tilts. The temporal standard deviation is plotted as a function of Mach number for each plate thickness in Fig. 12. In these plots, the blue line shows the spectrum of the baseline scenario where the turret was outside of the tunnel, with no excitation from the flow. The orange line shows the spectrum of the flow scenario where the turret was inside the wind tunnel and had both base motion and flow excitation. For the 1/4" plate case we see a clear increase in rms tilt between when the turret is in the test section vs when it is outside, with the latter having tilt ranging from 10 - 50 microradians of tilt while the tilt of the turret in the tunnel ranges from 30 - 190 microradians, showing that there is significant response of the turret to the unsteady pressure field. This difference between the turret being outside or inside the test section increases with flow speed. Note that the Mach 0.4 baseline case had corrupted data and was not included here. For the 1/2" plate case, as expected, the tilt seen for the turret either outside or inside the test section both baseline and flow was lower, ranging from 9 - 42 microradians for the turret inside the test section and 11 - 32 microradians for the turret outside the test section. For the

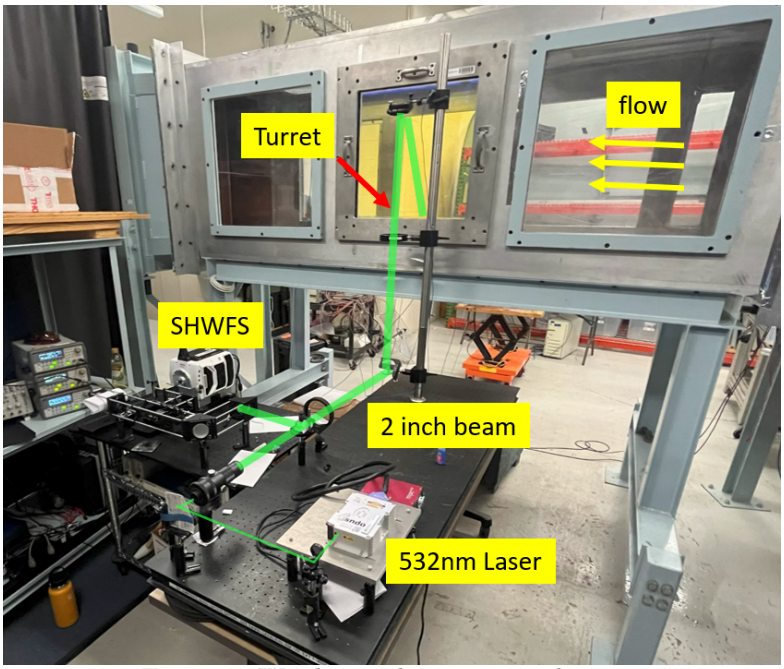


Figure 9: Wind tunnel experimental setup.



Figure 10: Turret installed outside of window tunnel to capture tunnel base vibration (left). Turret installed inside the wind tunnel at Azimuthal angle of 90 degrees(right).

lowest speed case, The tilt was actually higher tilt when the turret was outside of the test section. However, for the other speeds tested putting the turret in the flow increased rms tilt. For the 1" plate we see tilt values similar to the 1/2" plate ranging from 10 - 30 microradians for the the turret inside the test section and 11 - 20 microradians for the the turret outside the test section.

To further quantify the turret's vibration response, we plotted the tilt autospectra, which is shown for the 1/4" plate in Fig. 13 for Mach 0.2, 0.3, and 0.5 flow. The dashed vertical line shows the wind tunnel fan blade pass frequency. We can clearly see the 117 Hz and 220 Hz peaks corresponding to the drum and rocking vibration modes both when the turret is inside and outside the tunnel. These are the lowest frequency modes of the turret and therefore have the largest displacements. With the turret in the flow, there is a broadband increase in energy across all the frequencies, but for the Mach 0.5 case the 117 Hz peak does not grow very much compared to the rest of the spectra. Interestingly there is a hump in the baseline spectrum around 2000 Hz that seems to decrease when the turret is put in the flow. As the Mach number increases the peaks of the vibration

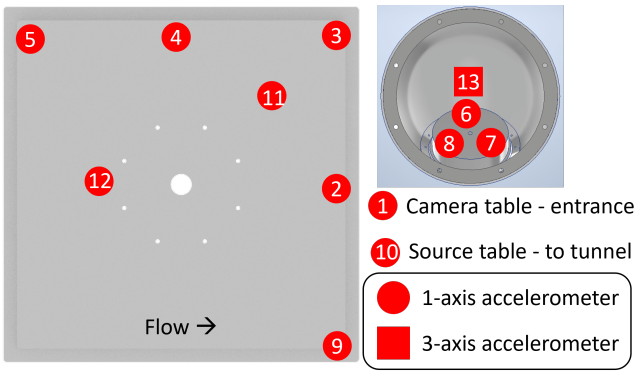


Figure 11: Location of accelerometers used for impact excitation testing. The canister is facing away from sensor 4.

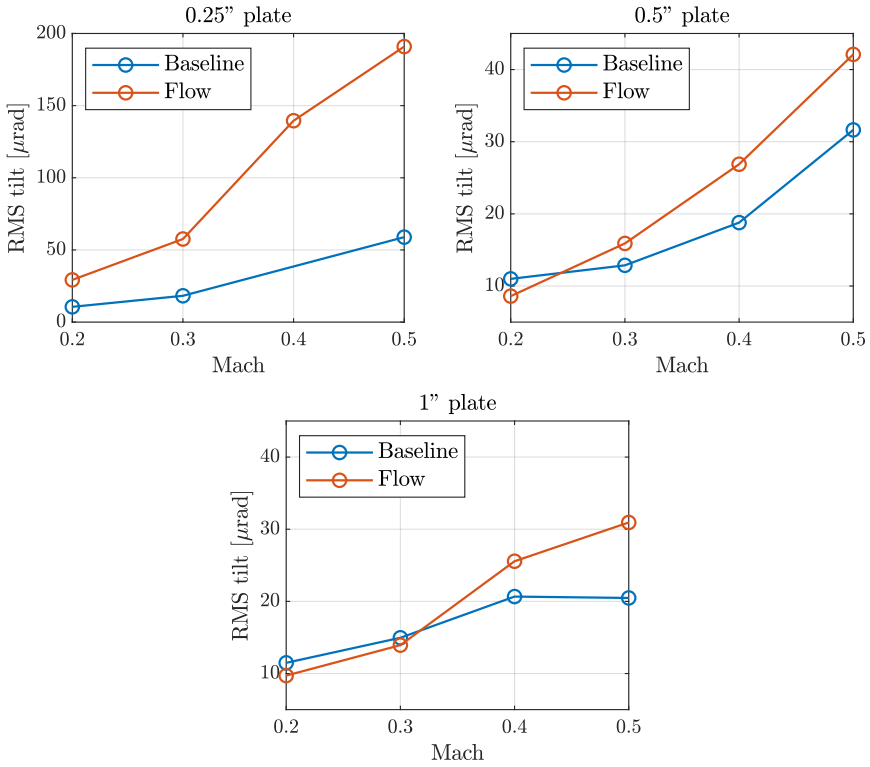


Figure 12: Rms of SHWFS measured global tilt of the turret on each plate for flow at different Mach numbers. Baseline case has the turret outside the tunnel so there is only base motion excitation. Flow case has turret inside the tunnel so there is both base motion and flow excitation.

modes become less defined for both cases. This could perhaps be due to the broadband spectrum of random fluctuations in the boundary layer. There may be added jitter from the optical access window vibrating. This was studied in depth for a similar setup using the same wind tunnel in Ref. 30

We can also see the influence of the very defined blade pass frequency in the data. For the Mach 0.2 case, the blade pass frequency aligns almost exactly with the 117 Hz mode which causes it to be very large, while for the Mach 0.3 case, the blade pass frequency is between the 117 Hz and 220 Hz modes and you can see a distinct third peak in the spectra. For the Mach 0.5 case the blade pass frequency is above the 220 Hz mode and we see a sharp peak. Harmonics of the blade pass are more distinct, such as in the Mach 0.2 case where there are very narrow peaks around 350 Hz and 470 Hz. Note that the blade pass frequency was slightly higher when the

turret was in the tunnel as having the turret in the flow creates blockage, requiring a higher fan speed to create the same flow speed. For the thicker plate cases taken after this, we decided to instead match the fan frequency between cases, as this is more important to the vibration environment, and the flow speed in the tunnel is likely not very important for the case when the turret is outside the tunnel.

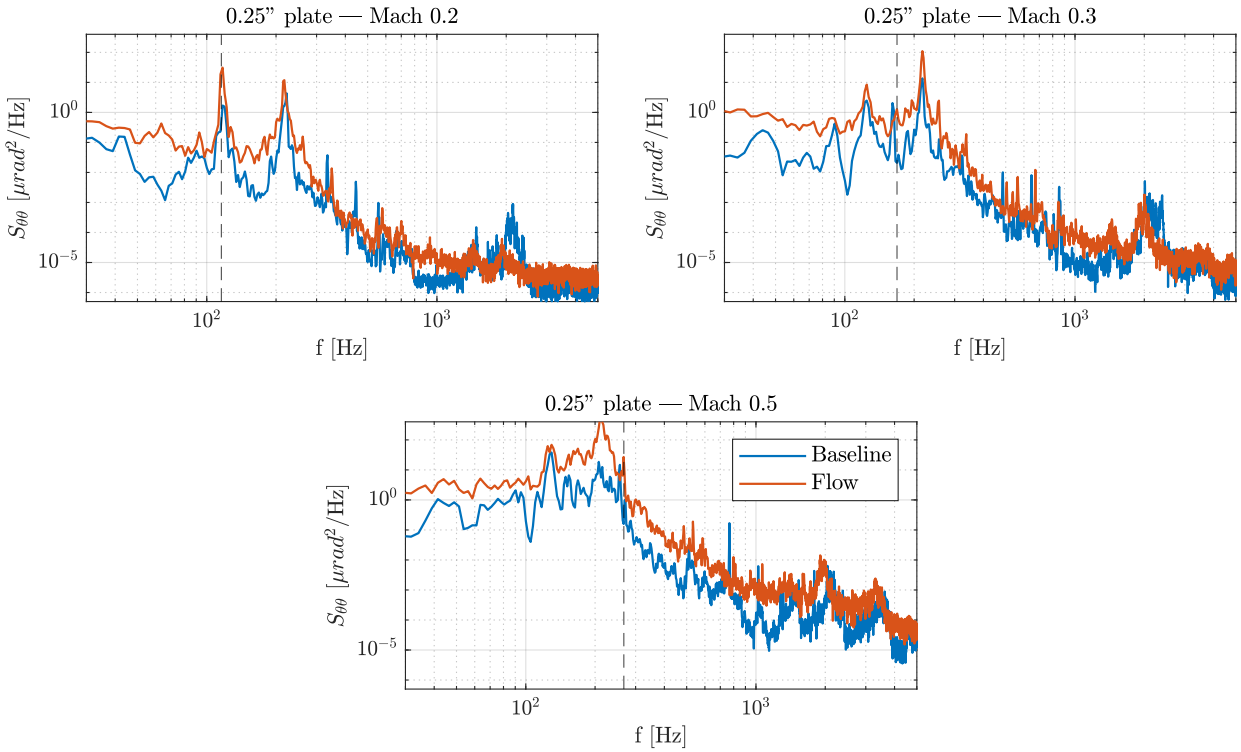


Figure 13: Spectra of SHWFS measured global tilt of the turret on 1/4" plate for flow at different Mach numbers. Baseline case has the turret outside the tunnel so there is only base motion excitation. Flow case has turret inside the tunnel so there is both base motion and flow excitation. Vertical dashed line shows wind tunnel fan blade pass frequency.

The autospectra for the 1/2" plate are shown in Fig. 14. These spectra look noticeably different than the 1/4" plate. We do not see any noticeable peaks at the vibration mode frequencies of 220 Hz and 440 Hz, but there is some concentration of energy in this region of frequencies. There is a slight peak at around 73 Hz, which is more pronounced for the baseline case and is lower for the flow case. For the Mach 0.2 case, this peak causes the rms tilt of the baseline case to be higher than the rms tilt when the turret is in the tunnel as seen in Fig. 12. The cause of this peak has not yet been fully determined, but could be a vibration mode associated with the wind tunnel test section and only shows up in the impact excitation tests when the turret is in the tunnel. It is unclear why it would decrease in energy when the turret is introduced into the flow. It also appears for the 1/4" plate case, however, in that case, the drumming and rocking modes are much stronger. The difference between the base motion only case and the case with the turret in the flow is much lower for the 1/2" plate than for the 1/4" plate. In Fig. 12, we saw that th

The autospectra for the 1" plate cases are shown in Fig. 15. Here we see results fairly similar to the 1/2" plate with the lower speed Mach 0.2 and 0.3 cases having similar tilt between the baseline case and the case with the turret in the tunnel. We see higher tilt for the baseline case at two peaks at 63 Hz and 80 Hz and over a band of frequencies from about 250 - 500 Hz. For the Mach 0.4 and 0.5 cases we see a larger separation between when the turret is inside vs outside the tunnel at the higher frequencies above 500 Hz. Similar to the 1/2" plate, the energy in the 60 - 80 Hz band is higher when the turret is outside of the wind tunnel and decreases when

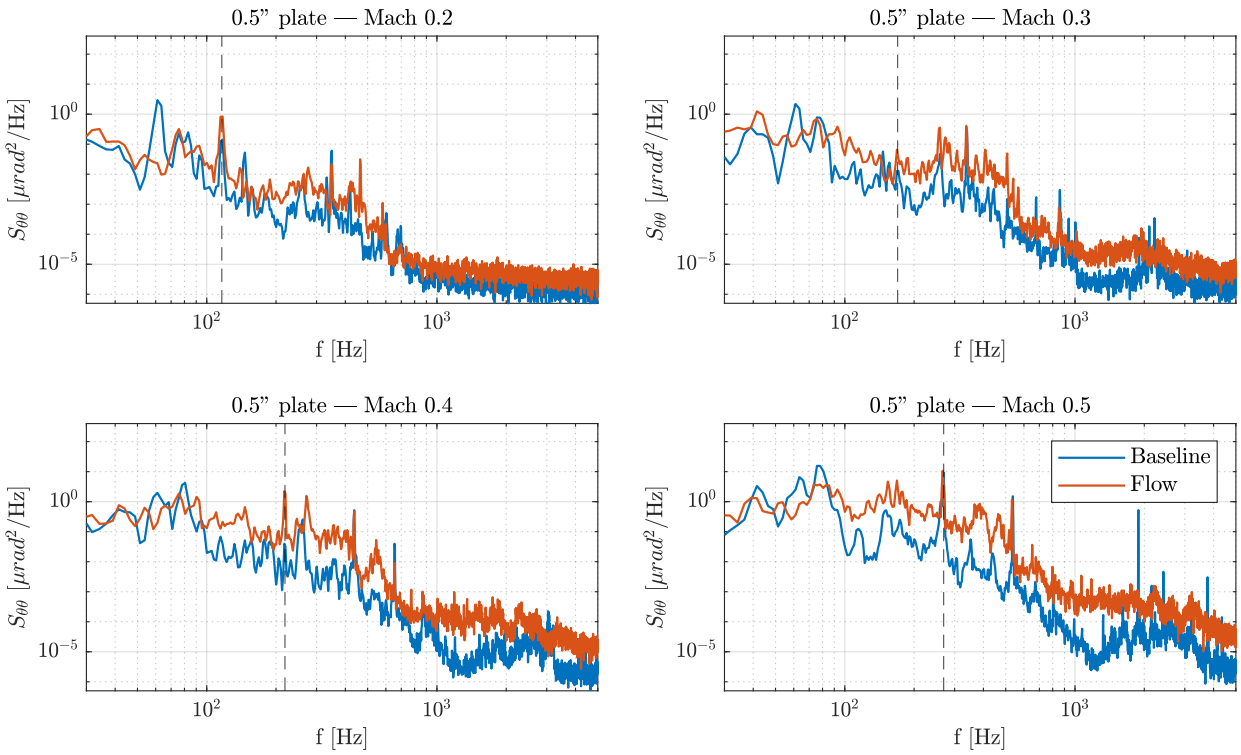


Figure 14: Spectra of SHWFS measured global tilt of the turret on 1/2” plate for flow at different Mach numbers. Baseline case has the turret outside the tunnel so there is only base motion excitation. Flow case has turret inside the tunnel so there is both base motion and flow excitation.Vertical dashed line shows wind tunnel fan blade pass frequency.

the turret is put into the flow. At the lower speeds of Mach 0.2 and 0.3, this leads to lower rms tilt values when the turret is in the flow compared to the baseline case as shown in Fig. 12. For the Mach 0.5 case, there is a broad peak around 170 Hz in the flow case that appears when the turret is in the flow, but not in the baseline. This would be around $St_D = 0.2$ and potentially could be a result of the flow-induced forcing. Further study is required. Overall, it seems that for the 1” plate majority of the tilt is coming from lower frequency modes, likely associated with tunnel features.

5. CONCLUSION

In the presented work, preliminary results were shown for work studying aero-mechanical jitter of a hemispherical optical turret. A simplified canonical geometry consisting of a hemispherical shell and canister to hold optics was designed to reduce the degrees of freedom and help better understand the fundamental physics, compared to the complicated prototype systems that have been studied in the past. Modal analysis of the turret and the plate that connects to the wind tunnel was performed in simulation through finite element analysis. The lowest frequency modes, which also exist in the range of frequencies of expected aerodynamic forcing, were found to have large displacements of the plate under the turret. The lowest frequency mode was a drumming mode where the center of the plate moves up and down. The next two modes were rocking modes which cause the canister to pitch and roll. Four higher frequency modes were shown in which the corners of the plate oscillate, but not much motion is imposed on the turret. Three plate thicknesses of 1/4”, 1/2”, and 1” were tested, all with the same mode shapes, but the thicker plates having higher natural frequencies. Impact excitation tests were performed to compare the manufactured turret and plates to simulation. For just the plate, the frequencies were found to match well, within 1%. For the plate and turret, measured modal frequencies were found to be within 3% for

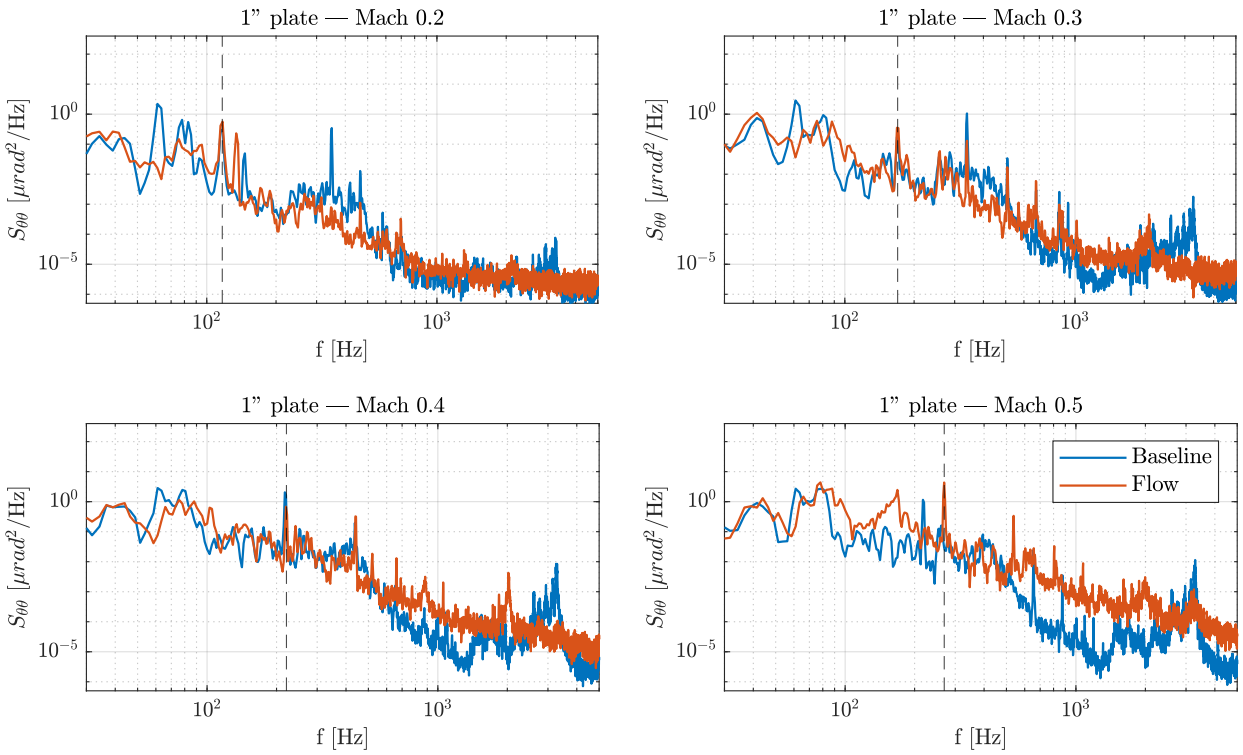


Figure 15: Spectra of SHWFS measured global tilt of the turret on 1" plate for flow at different Mach numbers. Baseline case has the turret outside the tunnel so there is only base motion excitation. Flow case has turret inside the tunnel so there is both base motion and flow excitation.Vertical dashed line shows wind tunnel fan blade pass frequency.

the 1/4" and 1/2" plates when using a free boundary condition. Agreement was worse for the 1" plate. Further investigation into model fidelity, accurate modeling of boundary conditions, etc. is underway. A spectral version of POD was used to separate and show vibration modes at a given frequency.

Wind tunnel measurements were then taken at the University of Notre Dame's White Field Mach 0.6 wind tunnel at speeds ranging from Mach 0.2 - 0.5. The turret and plate were instrumented with accelerometers and Shack–Hartmann tilt measurements were recorded. Two scenarios were tested: one with the turret inside the tunnel exposed to the flow, and another with the turret attached outside of the wind tunnel so that it is only excited by the base motion of the wind tunnel. For the thinnest 1/4" plate case, there was significantly more tilt when the turret was exposed to the flow with rms tilts ranging from 30 - 190 microradians for the speeds tested. The baseline case with the turret outside the tunnel only saw rms tilts between 10 - 50 microradians. The tilt spectra showed significant peaks at around 117 Hz and 220 Hz which correspond to the first two vibration modes. The blade pass frequency of the tunnel driver fan also had a significant influence which was apparent in the spectra. For the 1/2" plate the measured tilt was much lower than the 1/4" plate, ranging from 9 - 42 microradians for the turret in the flow and 11 - 32 microradians for the baseline case. In the autospectra there were not clear peaks at the vibration mode natural frequencies, but there was a broad hump in the range of frequencies between 220 - 600 Hz which is the range including the vibration modes. Overall for this thicker plate, there is less of a difference between the baseline case and when the turret is in the flow. For the thickest 1" plate the rms tilt was from 10 - 30 microradians for the flow and 11 - 20 microradians for the baseline. For the lower speeds, there was actually more tilt in the baseline case, than when the turret was in the flow. Again, the vibration mode frequencies have a broad hump in the autospectra, but not sharp peaks like for the 1/4" plate.

Overall, the simple turret model designed for this investigation only has three vibration modes which influence

tip tilt, along with potentially one low frequency mode from the wind tunnel test section. There is good spatial agreement between the modes measured in experiment and those calculated through finite element analysis. The natural frequencies are close, but more work needs to be done to update our model to get better agreement. Our wind tunnel results show that when the turret is exposed to flow, there is a clear increase in tilt compared to a baseline condition when only base motion of the wind tunnel excites vibration of the turret. Future work will be directed towards developing a better understanding of how the unsteady pressure field forcing relates to the beam jitter. This experimental work is also being compared with CFD-FEA simulations following the same geometry and flow conditions.

ACKNOWLEDGMENTS

This work is supported by the Air Force Research Lab, Cooperative agreement number FA9451-23-2-0016. The U.S. Government is authorized to reproduce and distribute reprints for governmental purposes notwithstanding any copyright notation thereon.

DISCLOSURES

The views expressed are those of the author and do not necessarily reflect the official policy or position of the Department of the Air Force, the Department of Defense, or the U.S. Government. Approved for public release; distribution is unlimited. Public Affairs release approval # AFRL-2024-4435

REFERENCES

[1] Ross, C. L., "Origins of the airborne laser," *Air Power History* **58**(1) (2011).

[2] Kyrazis, D. T., "Airborne Laser Laboratory departure from Kirtland Air Force Base and a brief history of aero-optics," *Optical Engineering* **52**(7), 1 – 6 (2012).

[3] Jumper, E. J., Zenk, M. A., Gordeyev, S. V., Cavalieri, D. A., and Whitely, M., "Airborne Aero-Optics Laboratory," *Optical Engineering* **52**(7), 1 – 12 (2013).

[4] Gordeyev, S., Jumper, E. J., and Whiteley, M., [*Aero-Optical Effects: Physics, Analysis and Mitigation*], Wiley (2023).

[5] Kalensky, M., Gordeyev, S., Kemnetz, M., and Spencer, M., "Aero-optical effects, part I. System-level considerations: tutorial," preprint on Optica Open at https://preprints.opticaopen.org/articles/preprint/Aero-optical_effects_part_I_System-level_considerations_tutorial/26142928 (July 2024).

[6] De Lucca, N. G., Gordeyev, S., Jumper, E. J., Hird, K., Juliano, T. J., Gregory, J., Thordahl, J., and Wittich, D. J., "The estimation of the unsteady aerodynamic force applied to a turret in flight," in [*44th AIAA Plasmadynamics and Lasers Conference*], San Diego, CA, AIAA Paper 2013-3136 (June 2013).

[7] Gordeyev, S., De Lucca, N., Jumper, E., Hird, K., Juliano, T., Gregory, J., Thordahl, J., and Wittich, D., "Comparison of unsteady pressure fields on turrets with different surface features using pressure-sensitive paint," *Experiments in Fluids* **55**(1) (2014).

[8] De Lucca, N. G., Gordeyev, S., Morrida, J. J., and Jumper, E. J., "Investigation of flow dynamics over turrets with different spanwise aspect ratios using psp," in [*2018 AIAA Aerospace Sciences Meeting*], Kissimmee, FL, AIAA Paper 2018-2047 (January 2018).

[9] Gordeyev, S., De Lucca, N. G., Morrida, J. J., and Jumper, E. J., "Conditional studies of the wake dynamics of hemispherical turret using psp," in [*2018 AIAA Aerospace Sciences Meeting*], Kissimmee, FL, AIAA Paper 2018-2048 (January 2018).

[10] Bukowski, T. J., Gordeyev, S., Kalensky, M., and Kemnetz, M. R., "Study of unsteady surface flowfields on and around turrets with different protrusions," *AIAA Journal* **61**(12), 5320–5331 (2023).

[11] De Lucca, N. G., Gordeyev, S. V., and Jumper, E. J., "In-flight aero-optics of turrets," *Optical Engineering* **52**(7), 1 – 14 (2013).

[12] Morrida, J. J., De Lucca, N. G., Gordeyev, S., and Jumper, E. J., "Simultaneous pressure and optical measurements around a hemispherical in subsonic and transonic flight," in [*AIAA Flight Testing Conference*], Denver, CO, AIAA Paper 2017-3654 (June 2017).

[13] Morrida, J., Gordeyev, S., De Lucca, N., and Jumper, E. J., "Shock-related effects on aero-optical environment for hemisphere-on-cylinder turrets at transonic speeds," *Appl. Opt.* **56**, 4814–4824 (Jun 2017).

[14] Malkus, M. J., Frede, M. T., Sherer, S. E., and Garmann, D. J., "Effect of submergence on transonic flow around a hemisphere," *AIAA Journal* **60**(11), 1–15 (2022).

[15] Jelic, R., Sherer, S., and Greendyke, R., "Simulation of various turrets at subsonic and transonic flight conditions using overflow," *Journal of Aircraft* **50**(2), 398–409 (2013).

[16] Gordeyev, S. and Jumper, E., "Fluid dynamics and aero-optics of turrets," *Progress in Aerospace Sciences* **46**(8), 388–400 (2010).

[17] Kalensky, M., *Airborne Measurement of Atmospheric-Induced Beam Jitter*, PhD thesis, University of Notre Dame (2022).

[18] Kemnetz, M. R., *Analysis of the Aero-Optical Component of the Jitter Using the Stitching Method*, PhD thesis, University of Notre Dame (2019).

[19] De Lucca, N., *Studies of the pressure field and related beam jitter for hemisphere-on-cylinder turrets*, PhD thesis, University of Notre Dame (2016).

[20] De Lucca, N. G., Gordeyev, S., and Jumper, E., "The study of aero-optical and mechanical jitter for flat window turrets," in [*50th AIAA Aerospace Sciences Meeting including the New Horizons Forum and Aerospace Exposition*], Nashville, TN, AIAA Paper 2012-0623 (January 2012).

[21] De Lucca, N. G., Gordeyev, S., and Jumper, E. J., "Effect of surface unsteady pressure field on global beam jitter for a hemisphere-on-cylinder turret," in [*52nd Aerospace Sciences Meeting*], National Harbor, MD, AIAA Paper 2014-0322 (January 2014).

[22] Merritt, P. and Sher, L., "Summary of aerodynamic vibration effects on an airborne turret," in [*Aero-Optical Phenomena*], Gilbert, K. G. and Otten, L. J., eds., **80**, 343–356, American Institute of Aeronautics and Astronautics (January 1982).

[23] Griffin, S. F. and Kelchner, B. L., "Line-of-sight jitter for advanced tactical laser," *AIAA Journal* **61**(7), 3204–3209 (2023).

[24] Merritt, P. and Spencer, M., [*Beam Control for Laser Systems*], ch. 3. System Engineering, Performance Equations, and Error Budgets, 84–87, The Directed Energy Professional Society (2018).

[25] Roeder, A. L. and Gordeyev, S., "Wake response downstream of a spanwise-oscillating hemispherical turret," *Journal of Fluids and Structures* **109**, 103470 (2022).

[26] Kalensky, M., Catron, B., Gordeyev, S. V., Jumper, E. J., and Kemnetz, M., "Investigation of aero-mechanical jitter on a hemispherical turret," in [*Proceedings of SPIE*], Dolne, J. J. and Spencer, M. F., eds., SPIE (August 2021).

[27] Griffin, S., Blackburn, J., Wittich, J., Gordeyev, S., and Jumper, E. J., "Integrated line-of-sight modeling of the airborne aero-optics laboratory," in [*Proceedings of the Advanced Maui Optical and Space Surveillance Technologies Conference*], Ryan, S., ed. (September 2013).

[28] Towne, A., Schmidt, O. T., and Colonius, T., "Spectral proper orthogonal decomposition and its relationship to dynamic mode decomposition and resolvent analysis," *Journal of Fluid Mechanics* **847**, 821–867 (2018).

[29] Schmidt, O. T. and Towne, A., "An efficient streaming algorithm for spectral proper orthogonal decomposition," *Computer Physics Communications* **237**, 98–109 (2019).

[30] De Lucca, N. G., Gordeyev, S., Smith, A. E., Jumper, E. J., Whiteley, M., and Neale, T., "The removal of tunnel vibration induced corruption in aero-optical measurements," in [*45th AIAA Plasmadynamics and Lasers Conference*], American Institute of Aeronautics and Astronautics (June 2014).